JOURNAL OF APPLIED ELECTROCHEMISTRY **27** (1997) 529–538

Cathodic polarization of copper electrode in CuCN–KCN solutions and the current distribution for copper deposition on grooved substrates

A. KATAGIRI

Chemistry Laboratory, Faculty of Integrated Human Studies, Kyoto University, Sakyo-ku, Kyoto 606, Japan

H. INOUE, N. OGURE

Ebara Corporation, Fujisawa, Kanagawa 251, Japan

Received 28 March 1996; revised 7 October 1996

The cathodic polarization of a copper electrode in CuCN/KCN solution was interpreted by considering the diffusion and migration of all ionic species, chemical reactions involving cyano-copper(I) complexes, and the quasiequilibrium of charge transfer reaction. Experimental polarization curves were compared with theoretical ones, where the diffusion layer thickness was determined. The present model was applied to the prediction of thickness distribution of copper coating on grooved substrates. Two types of substrates with grooves of different size (width × depth), (**a**) 5 mm × 5 mm and (**b**) 1 mm × 1 mm, were used. Agreement between theory and experiment was satisfactory for substrate **a**, but not for substrate **b**. The effect of convective mass transfer in the groove was discussed.

List of symbols

c	concentration
d	thickness of diffusion layer
D	diffusion coefficient
E	electrode potential
F	Faraday constant
i	current density
i_0	exchange current density
I	ionic strength
$\boldsymbol{j}_i$	flux of species i
J	dimensionless current
T	absolute temperature
z_i	charge number of species i
β	overall formation constant (in terms of concentrations)
β^a	overall formation constant (in terms of activities)
ϕ	electric potential in solution

Superscript

0	bulk of solution

Subscripts

m	Cu $(CN)_m^{(m-1)-}$ ion ($m = 2, 3, 4$)
CN	CN^- ion
A	total cyanide ion
M	total copper ion
S	K^+ ion

1. Introduction

Copper plating in a cyanide bath is a widely used industrial process. Although the importance of current distribution is well recognized in determining uniform and coherent deposits [1–3], few basic researches have been reported on copper deposition from cyanide solutions. Current distribution is particularly important in fabrication of microelectronic devices.

Qualitative explanation has been given to the polarization phenomena in copper deposition from cyanide solutions [4–6]. Glasstone [4] examined the equilibrium potential of copper as a function of the CN/Cu ratio, that is, the ratio of the total cyanide concentration (c_A) to the total copper concentration (c_M), and considered that the complex ions $Cu(CN)_2^-$ and $Cu(CN)_3^{2-}$ can both exist. From the observations that stirring has a significant effect in reducing cathodic polarization, he concluded that both complex ions dissociate rapidly. It was supposed that stirring retards the increase of the CN/Cu ratio at the cathode. Kuwa *et al.* [5, 6] measured cathodic polarization under a large variety of conditions. They considered that a kind of concentration polarization occurs due to the liberation of CN^- ions in the electrode reaction.

$$Cu(CN)_2^- + e^- \rightarrow Cu + 2CN^- \qquad (1)$$

Gerischer [7, 8] investigated the charge-transfer kinetics of metal deposition from complex electrolyte solutions by potentiostatic and a.c. impedance measurements. In [7], he referred to a possible effect of the concentration change of ligand anion on cathodic

0021-891X

polarization. Costa [9] performed detailed investigation on the kinetics of copper deposition by a rapid potentiostatic method and a galvanostatic double pulse method. He reported a stationary current–potential curve which showed characteristics of diffusion phenomena: the charge transfer coefficient was too small ($\alpha = 0.032$), and dependent on stirring. Bek and Zhukov [10] discussed cathodic polarization taking into account the diffusion and chemical equilibria of different cyano-copper(I) complexes. In the theoretical modelling of pulse plating of copper-containing alloys, Ruffoni and Landolt [12] referred to the role of the cyanide ions liberated at the cathode. However, there has not been a theoretical treatment of concentration polarization which takes into account the diffusion, migration, and chemical reactions at the cathode.

In a previous paper [13], a numerical method was proposed for calculating steady-state current distribution which is controlled by diffusion and migration of ions. Thus, diffusion–migration equations for all ions were combined with a differential equation which, at steady state, reduces to Poisson's equation. As reported in preliminary papers [14, 15], this method can be applied to copper deposition from cyanide solutions.

The present paper describes a theoretical treatment of polarization in copper deposition and its application to the thickness distribution of copper deposit on grooved substrates.

2. Equilibrium potential of copper electrode

To discuss the concentration polarization at the cathode, we first consider the equilibrium potential of a copper electrode in a cyanide bath which is prepared from CuCN and KCN. Assuming equilibria involving three types of cyano complexes,

$$Cu^+ + 2CN^- = Cu(CN)_2^- \tag{2}$$

$$Cu^+ + 3CN^- = Cu(CN)_3^{2-} \tag{3}$$

$$Cu^+ + 4CN^- = Cu(CN)_4^{3-} \tag{4}$$

the concentration of each copper species, in M ($\mathrm{mol\,dm^{-3}}$), can be expressed as

$$[Cu^+] = c_M / \left(1 + \beta_2[CN^-]^2 + \beta_3[CN^-]^3 + \beta_4[CN^-]^4\right) \tag{5}$$

$$\left[Cu(CN)_m^{(m-1)-}\right] = c_M \beta_m [CN^-]^m / \left(1 + \beta_2[CN^-]^2 + \beta_3[CN^-]^3 + \beta_4[CN^-]^4\right) \quad (m = 2,\ 3,\ 4) \tag{6}$$

where β_m is the overall formation constant of $Cu(CN)_m^{(m-1)-}$ in terms of concentrations. Figure 1 shows concentration of each copper species which is calculated from Equations 5 and 6 using literature values of $\beta_2^a = 1 \times 10^{24}$, $\beta_3^a = 3.8 \times 10^{28}$, and $\beta_4^a = 2 \times 10^{30}$ (in terms of activities) [16] for β_2, β_3, and β_4 at 25 °C. The CN/Cu ratio is written as

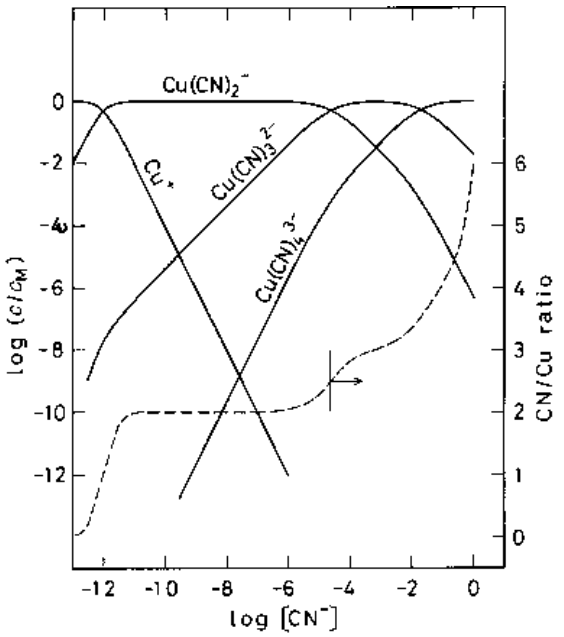

Fig. 1. Logarithms of relative concentrations of different copper species as functions of log [CN^-]. The CN/Cu curve (broken line) was calculated for $c_M = 0.5$ M.

$$\frac{c_A}{c_M} = \frac{[CN^-]}{c_M} + \frac{2\beta_2[CN^-]^2 + 3\beta_3[CN^-]^3 + 4\beta_4[CN^-]^4}{1 + \beta_2[CN^-]^2 + \beta_3[CN^-]^3 + \beta_4[CN^-]^4} \tag{7}$$

If c_M is given, Equation 7 determines the CN/Cu ratio as a function of [CN^-]. The broken line in Fig. 1 illustrates such a relationship for $c_M = 0.5$ M. Since the CN/Cu ratio is usually greater than 2.5 in practical plating baths, the copper species which can exist in significant concentrations are $Cu(CN)_2^-$, $Cu(CN)_3^{2-}$, and $Cu(CN)_4^{3-}$. (Cu^+ can be neglected.)

The Nernst equation for the copper electrode is given as

$$E = E^\circ + (RT/F)\ln a_{Cu^+} = E^\circ + (RT/F)\ln \gamma_{Cu^+} + (RT/F)\ln [Cu^+] \tag{8}$$

where E° is the standard electrode potential and γ_{Cu^+} is the activity coefficient of Cu^+ ion. Introducing Equation 5 into Equation 8 and using the formal electrode potential $E^{\circ\prime} = E^\circ + (RT/F)\ln \gamma_{Cu^+}$, the following equation can be derived.

$$E = E^{\circ\prime} + (RT/F)\ln\left\{c_M/(1 + \beta_2[CN^-]^2 + \beta_3[CN^-]^3 + \beta_4[CN^-]^4)\right\} \tag{9}$$

If c_M is given, E can be calculated as a function of [CN^-]. Thus Equations 7 and 9 determine the relationship between E and c_A/c_M, where [CN^-] is an intermediate variable.

Figure 2 shows experimental and theoretical relationships between E and c_A/c_M under three different conditions. In theoretical calculations, values of β_n at temperature T and at ionic strength I were estimated from the enthalpies of reactions (Appendix A) and activity coefficients of ions (Appendix B). The

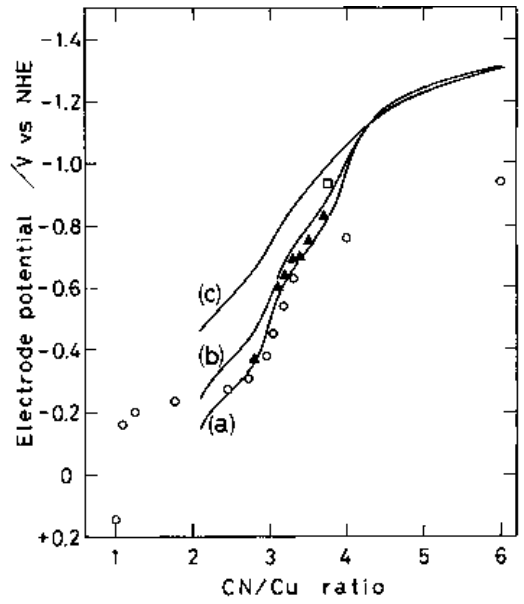

Fig. 2. Equilibrium potential of a copper electrode in cyanide solutions. Theoretical curves were obtained from Equations 7 and 9 for $c_M = 0.5$ M at (a) 15 °C, (b) 30 °C and (c) 60 °C. Experimental data are shown by: (○) Glasstone [4], 15 °C, (▲) Kuwa *et al.* [5], 30 °C, and (□) present work, 60 °C.

theoretical curves are substantially in accord with experimental data. When a cathodic current is passed, the CN/Cu ratio at the electrode surface increases due to the liberation of cyanide ions from cyano-copper complexes, and therefore the electrode potential shifts in the negative direction. Thus, concentration polarization occurs. For detailed analysis mass transfer of all species as well as chemical reactions in the diffusion layer must be considered.

3. Concentration and potential distributions and polarization curves

We assume a stagnant region near the cathode and consider diffusion and migration of K^+, CN^-, $Cu(CN)_2^-$, $Cu(CN)_3^{2-}$, and $Cu(CN)_4^{3-}$, and the following chemical reactions:

$$Cu(CN)_2^- + CN^- \xrightarrow{v_a} Cu(CN)_3^{2-} \quad (10)$$

$$Cu(CN)_3^{2-} + CN^- \xrightarrow{v_b} Cu(CN)_4^{3-} \quad (11)$$

Here v_a and v_b represent the net rates of reactions which are functions of location and time. Using subscripts S, CN, 2, 3, and 4 for K^+, CN^-, $Cu(CN)_2^-$, $Cu(CN)_3^{2-}$, and $Cu(CN)_4^{3-}$, respectively, the rates of changes of concentrations are given as

$$\partial c_S/\partial t = -\nabla\cdot\boldsymbol{j}_S \quad (12)$$

$$\partial c_{CN}/\partial t = -\nabla\cdot\boldsymbol{j}_{CN} - v_a - v_b \quad (13)$$

$$\partial c_2/\partial t = -\nabla\cdot\boldsymbol{j}_2 - v_a \quad (14)$$

$$\partial c_3/\partial t = -\nabla\cdot\boldsymbol{j}_3 + v_a - v_b \quad (15)$$

$$\partial c_4/\partial t = -\nabla\cdot\boldsymbol{j}_4 + v_b \quad (16)$$

where $\boldsymbol{j}_i$ is the flux of species i [1]. When ions move by migration and diffusion, $\boldsymbol{j}_i$ is expressed by

$$\boldsymbol{j}_i = -(z_i F D_i c_i/RT)\nabla\phi - D_i\nabla c_i \quad (17)$$

where z_i is the charge number of species i, D_i is the diffusion coefficient and ϕ is the electric potential in the solution. Eliminating v_a and v_b from Equations 13–16, the following differential equations can be derived:

$$\partial(c_2 + c_3 + c_4)/\partial t = -\nabla\cdot(\boldsymbol{j}_2 + \boldsymbol{j}_3 + \boldsymbol{j}_4) \quad (18)$$

$$\partial(c_{CN} + 2c_2 + 3c_3 + 4c_4) = -\nabla\cdot(\boldsymbol{j}_{CN} + 2\boldsymbol{j}_2 + 3\boldsymbol{j}_3 + 4\boldsymbol{j}_4) \quad (19)$$

It is convenient to use c_M and c_A as additional variables.

$$c_M = c_2 + c_3 + c_4 \quad (20)$$

$$c_A = c_{CN} + 2c_2 + 3c_3 + 4c_4 \quad (21)$$

Combination of Equations 12, 17–21 yields

$$\partial c_S/\partial t = (F/RT)\nabla\cdot(D_S c_S\nabla\phi) + \nabla\cdot D_S\nabla c_S \quad (22)$$

$$\partial c_M/\partial t = -(F/RT)\nabla\cdot\{(D_2c_2 + 2D_3c_3 + 3D_4c_4)\nabla\phi\} + \nabla\cdot(D_2\nabla c_2 + D_3\nabla c_3 + D_4\nabla c_4) \quad (23)$$

$$\partial c_A/\partial t = -(F/RT)\nabla\cdot\{(D_{CN}c_{CN} + 2D_2c_2 + 6D_3c_3 + 12D_4c_4)\nabla\phi\} + \nabla\cdot(D_{CN}\nabla c_{CN} + 2D_2\nabla c_2 + 3D_3\nabla c_3 + 4D_4\nabla c_4) \quad (24)$$

If we assume equilibria of Reactions 10 and 11, concentrations c_{CN}, c_2, c_3 and c_4 are related by

$$c_3/c_2c_{CN} = K_3 \quad (25)$$

$$c_4/c_3c_{CN} = K_4 \quad (26)$$

where K_3 and K_4 are the consecutive formation constants of $Cu(CN)_3^{2-}$ and $Cu(CN)_4^{3-}$, respectively ($K_3 = \beta_3/\beta_2, K_4 = \beta_4/\beta_3$). The potential in the solution obeys Poisson's equation

$$\nabla^2\phi = -(F/\varepsilon)(c_S + c_M - c_A) \quad (27)$$

where ε is the dielectric constant of the solution. As described in the previous paper [13], we can postulate a differential equation

$$\partial\phi/\partial t = \alpha\left\{\nabla^2\phi + (F/\varepsilon)(c_S + c_M - c_A)\right\} \quad (28)$$

in which α is a hypothetical constant. Equation 28 reduces to Poisson's equation at steady state ($\partial\phi/\partial t = 0$). The partial differential equations (Equations 22–24 and 28) can be transformed to the corresponding difference equations, which, in combination with Equations 20, 21, 25 and 26, can be solved numerically to give steady-state values of c_S, c_M, c_A, c_{CN}, c_2, c_3, c_4 and ϕ.

Boundary conditions at the electrode surface under a constant current can be formulated as follows. Since K^+ and CN^- do not move across the electrode–electrolyte interface, the flux of K^+ and the total flux of cyanide in the direction (n) normal to the electrode surface are zero. Thus,

$$-(FD_S c_S/RT)\partial\phi/\partial n - D_S \partial c_S/\partial n = 0 \quad (29)$$

$$(F/RT)(D_{CN}c_{CN} + 2D_2c_2 + 6D_3c_3 + 12D_4c_4)\partial\phi/\partial n - (D_{CN}\partial c_{CN}/\partial n + 2D_2\partial c_2/\partial n + 3D_3\partial c_3/\partial n + 4D_4\partial c_4/\partial n) = 0 \quad (30)$$

The total flux of copper at the electrode surface is related to the current density i:

$$i = \{(D_2c_2 + 2D_3c_3 + 3D_4c_4)/RT\}\partial\phi/\partial n - (D_2\partial c_2/\partial n + D_3\partial c_3/\partial n + D_4\partial c_4/\partial n)/F \quad (31)$$

The equation of electroneutrality can be used as the fourth boundary condition:

$$c_S + c_M - c_A = 0 \quad (32)$$

Equations 20, 21, 25, 26 and 29–32 determine the values of eight variables (c_S, c_M, c_A, c_{CN}, c_2, c_3, c_4 and ϕ) at the electrode surface.

For simplicity all the D_i values are assumed to be identical ($D_i = D$). It is convenient to use the following dimensionless quantities:

$$C_M = c_M/c_M^0,\ C_A = c_A/c_M^0,\ C_S = c_S/c_M^0,\ \Phi = F\phi/RT,\ J = il/FDc_M^0 \quad (33)$$

Here c_M^0 is the bulk concentration of total copper and l is the characteristic length. In later discussion, l is represented by the thickness of diffusion layer d in the one-dimensional case, and by the width of a groove in the two-dimensional case.

Figure 3 shows an example of one-dimensional distributions of concentrations (solid lines) and potential (broken line) calculated for $c_M^0 = 0.08$ M, $c_A^0 = 0.18$ M, $c_S^0 = 0.1$ M (the composition used by Glasstone [4]), $T = 288$ K, and $J = 0.5$. The distance x is taken from the surface of the electrode. It can be seen that free CN^- ions and copper complexes with larger CN^- coordination numbers accumulate near the electrode.

Figure 4 is another example for $c_M^0 = 0.56$ M, $c_A^0 = 2.10$ M, $c_S^0 = 1.54$ M (the composition of CuCN 50 g dm^{-3} and KCN 100 g dm^{-3}), $T = 333$ K, and $J = 0.5$. It is noted that the current causes only small potential difference (a few mV) across the diffusion layer.

Assuming the quasiequilibrium of charge-transfer reaction, the electrode potential can be calculated by introducing the values of c_M and c_{CN} (=[CN^-]) at $x = 0$ into Equation 9. Thus the results of Figs 3 and 4 yield $E = -0.997$ V and -1.334 V, respectively. Concentration overpotential, that is, the shift of E from the equilibrium potential ($E_{eq} = -0.387$ V and -1.005 V, respectively) is significant. The validity of the quasiequilibrium of charge-transfer reaction will be examined in the following section.

By repeating the above calculations for different currents we can obtain theoretical current–potential curves. Figure 5 illustrates four examples of theoretical polarization curves for combinations of $c_A^0/c_M^0 = 2.25$ and 3.75, and $T = 288$ K and 333 K. Curves (a)–(c) exhibit a plateau which was sometimes observed in polarization measurements [4–6, 10]. Curves (c) and (d) correspond to the present work, which will be described in the following section. In a region between $J = 0.1$ and 0.6, curve (d) can be approximated by the following empirical equation:

$$E = -0.34 \log J - 1.44 \quad (34)$$

The apparent Tafel slope (0.34 V decade^{-1}) is much larger than that for simple charge-transfer overpotential (typically 0.12 V decade^{-1} for a one-electron reaction). Such a large Tafel slope was also reported by Costa [9].

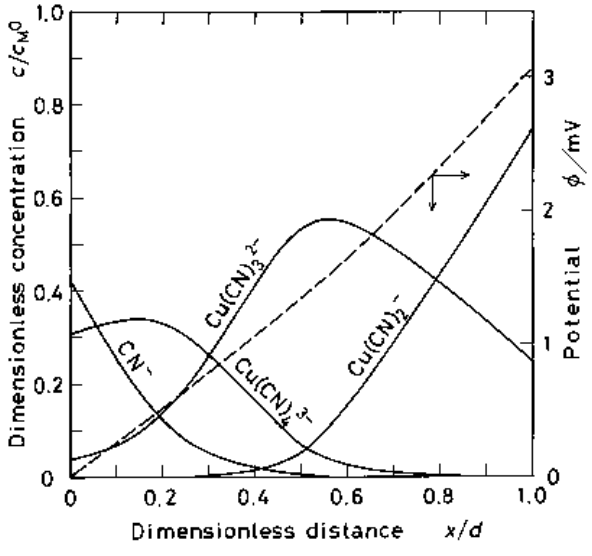

Fig. 3. One-dimensional distributions of concentrations and potential in the diffusion layer. $c_M^0 = 0.08$ M, $c_A^0 = 0.18$ M, $c_S^0 = 0.1$ M (the composition used by Glasstone [4]), $T = 288$ K, $\beta_2 = 1.1 \times 10^{24}$, $\beta_3 = 2.0 \times 10^{28}$, $\beta_4 = 5.0 \times 10^{30}$, $id/FDc_M^0 = 0.5$.

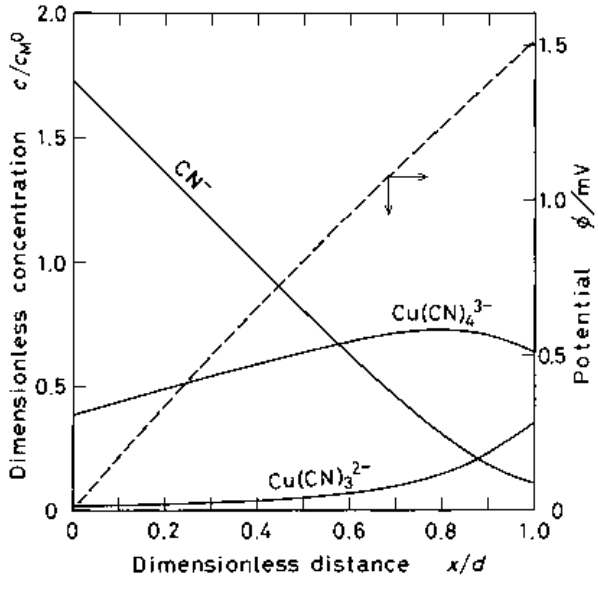

Fig. 4. One-dimensional distributions of concentrations and potential in the diffusion layer. $c_M^0 = 0.56$ M, $c_A^0 = 2.10$ M, $c_S^0 = 1.54$ M (the composition used in the present work), $T = 333$ K, $\beta_2 = 1.8 \times 10^{22}$, $\beta_3 = 3.8 \times 10^{25}$, $\beta_4 = 1.1 \times 10^{27}$, $id/FDc_M^0 = 0.5$.

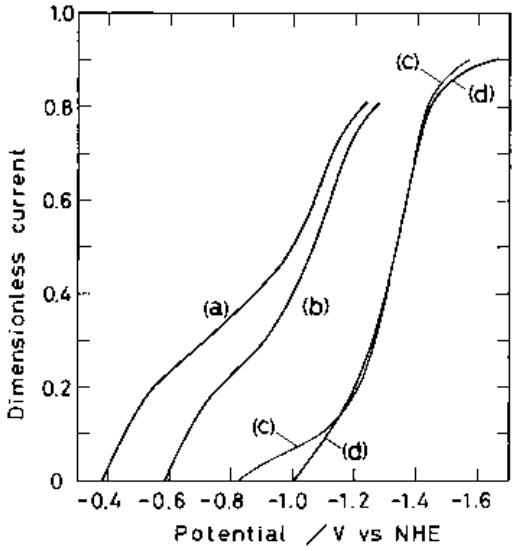

Fig. 5. Theoretical polarization curves for the copper cathode in cyanide solutions. (Curve a) $c_M^0 = 0.08$ M, $c_A^0 = 0.18$ M, $c_S^0 = 0.1$ M, $T = 288$ K, $\beta_2 = 1.1 \times 10^{24}$, $\beta_3 = 2.0 \times 10^{28}$, $\beta_4 = 5.0 \times 10^{30}$, $E^{0'} = 0.514$ V; (curve b) $c_M^0 = 0.08$ M, $c_A^0 = 0.18$ M, $c_S^0 = 0.1$ M, $T = 333$ K, $\beta_2 = 5.4 \times 10^{22}$, $\beta_3 = 9.3 \times 10^{25}$, $\beta_4 = 1.4 \times 10^{27}$, $E^{0'} = 0.509$ V; (curve c) $c_M^0 = 0.56$ M, $c_A^0 = 2.10$ M, $c_S^0 = 1.54$ M, $T = 288$ K, $\beta_2 = 3.8 \times 10^{23}$, $\beta_3 = 8.8 \times 10^{27}$, $\beta_4 = 4.0 \times 10^{30}$, $E^{0'} = 0.501$ V; (curve d) $c_M^0 = 0.56$ M, $c_A^0 = 2.10$ M, $c_S^0 = 1.54$ M, $T = 333$ K, $\beta_2 = 1.8 \times 10^{22}$, $\beta_3 = 3.8 \times 10^{25}$, $\beta_4 = 1.1 \times 10^{27}$, $E^{0'} = 0.494$ V.

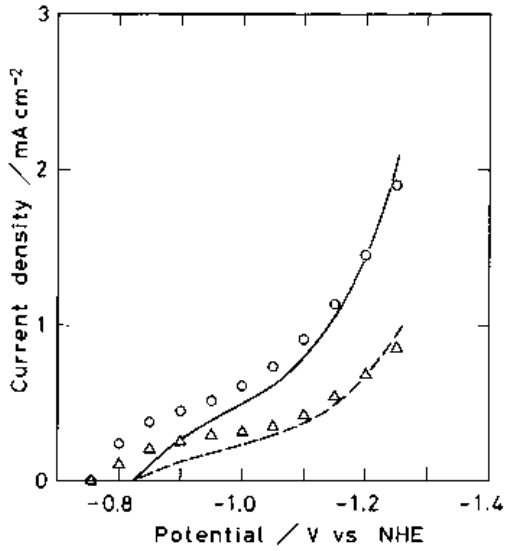

Fig. 6. Current–potential relationship for the copper cathode in a cyanide solution. CuCN 50 g dm^{-3}, KCN 100 g dm^{-3} ($c_M = 0.56$ M, $c_A = 2.10$ M, $c_S = 1.54$ M); temperature, 15 °C. The experimental data were obtained in stirred (○) and unstirred (△) solutions. The theoretical curves were drawn for $D/d = 1.4 \times 10^{-4}$ cm s^{-1} (——) and $D/d = 0.66 \times 10^{-4}$ cm s^{-1} (- - - -).

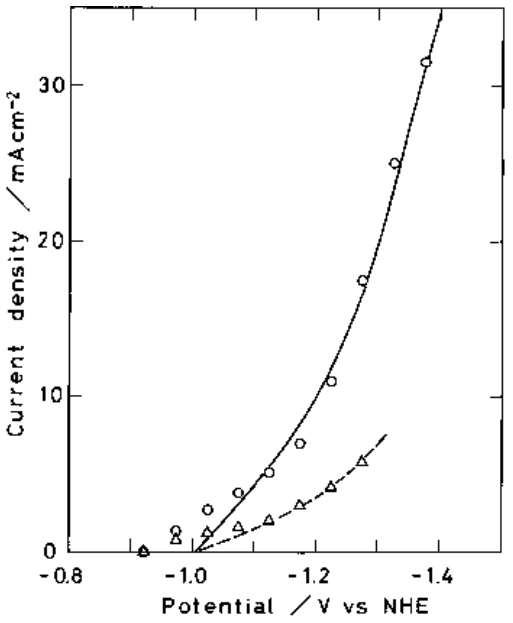

Fig. 7. Current–potential relationship for the copper cathode in a cyanide solution. CuCN 50 g dm^{-3}, KCN 100 g dm^{-3} ($c_M = 0.56$ M, $c_A = 2.10$ M, $c_S = 1.54$ M); temperature, 60 °C. The experimental data were obtained in stirred (○) and unstirred (△) solutions. The theoretical curves were drawn for $D/d = 9.2 \times 10^{-4}$ cm s^{-1} (——) and $D/d = 3.2 \times 10^{-4}$ cm s^{-1} (- - - -).

4. Experimental polarization curves

Steady-state current potential characteristics for copper deposition were measured in stirred and unstirred solutions at 15 °C and 60 °C. The electrode was a copper plate (10 mm × 20 mm), the reverse side of which was insulated by silicone rubber; effective electrode area = 2 cm^2. The electrolyte solution was prepared by dissolving CuCN (50 g dm^{-3}) and KCN (100 g dm^{-3}) in water. The conductivity of the solution was $\kappa = 0.106$ S cm^{-1} at 15 °C and $\kappa = 0.195$ S cm^{-1} at 60 °C. An H-shaped Pyrex cell with a glass frit separator was used. The working electrode compartment was 45 mm in diameter and contained 100 cm^3 of solution. The solution was stirred magnetically with a 30 mm magnet bar which rotated at about 300 rpm at the position 2 cm below the electrode. The electrode potential was measured against a saturated calomel electrode which was connected to the solution with a Luggin capillary. The estimated ohmic potential drop in the solution (~2 mm) between the electrode and the tip of the Luggin capillary was small (0.02 V at a current density of 10 mA cm^{-2} at 15 °C), and therefore, neglected.

Figures 6 and 7 show the results obtained in stirred (○) and unstirred (△) solutions. The solid and broken lines are theoretical ones which will be described in the following paragraph. The polarization characteristics is similar to that reported by Glasstone [4] and Kuwa *et al.* [5, 6] and Bek and Zhukov [10]. The marked effect of stirring indicates that the mass transfer controls the current. The magnitude of charge-transfer overpotential can be estimated from the kinetic data obtained by Costa [9]. He reported, for example, an exchange current density of $i_0 = 19$ mA cm^{-2} for $c_M = 0.08$ M and $c_A = 0.33$ M at 31 °C. The approximate linear expression of charge-transfer overpotential [17]

$$\eta = (RT/F)(i/i_0) \qquad (35)$$

gives the value of $\eta = 14$ mV at the current density of 10 mA cm^{-2} (the average current density used in the present work). Costa observed positive dependence of i_0 upon c_M and c_A, and therefore η should be much smaller than 14 mV for $c_M = 0.56$ M and $c_A = 2.10$ M. He also studied the temperature dependence of i_0 and

obtained the activation energy of $31\,kJ\,mol^{-1}$, which predicts $i_0(15\,^\circ C)/i_0(31\,^\circ C) \approx 0.5$ and $i_0(60\,^\circ C)/i_0(31\,^\circ C) \approx 3$. Therefore, the charge-transfer overpotential for $c_M = 0.56\,M$ and $c_A = 2.10\,M$ at $10\,mA\,cm^{-2}$ should be much smaller than 28 mV and 5 mV at 15 °C and 60 °C, respectively. It can be neglected in discussing the observed overpotential which was as large as 0.3 V at $10\,mA\,cm^{-2}$ even in stirred solution.

The experimental data of Fig. 6 can be compared with the theoretical calculation (curve (c) in Fig. 5). Best fitting yields the values of $D/d = 1.4 \times 10^{-4}\,cm\,s^{-1}$ and $0.66 \times 10^{-4}\,cm\,s^{-1}$ in stirred and unstirred solutions, respectively. Since D is estimated to be $4.7 \times 10^{-6}\,cm^2 s^{-1}$ (see Appendix C), values of $d = 0.033$ cm and 0.071 cm are derived in stirred and unstirred solutions, respectively. The solid and broken lines in Fig. 6 are the corresponding theoretical curves. The theoretical curves show characteristics similar to the experimental data, but the agreement is not very good at less negative potentials. This may be caused by possible errors in estimating β_m values.

The experimental data of Fig. 7 can be compared with the theoretical calculation (curve (d) in Fig. 5). Least squares fitting above 1.1 V yields $D/d = 9.2 \times 10^{-4}\,cm\,s^{-1}$ and $3.2 \times 10^{-4}\,cm\,s^{-1}$ for stirred and unstirred solutions, respectively. The solid and broken lines show the theoretical polarization curves. Poor agreement at less negative potentials may be due to errors in β_m. Estimated values of $D = 1.03 \times 10^{-5}\,cm^2\,s^{-1}$ gives $d = 0.011$ cm and 0.032 cm for stirred and unstirred solutions, respectively.

5. Copper plating on grooved substrates

The above modelling was applied to copper deposition on grooved substrates. Thus the thicknesses of copper coating on two types of substrates were measured and compared with theoretical calculations.

5.1. *Experimental details*

Copper plating bath was prepared in the same way as described above. The substrates (cathode) were steel plates (SS41) on which parallel grooves were precisely machined. Figure 8 shows one type of substrate (**a**) having parallel grooves which were 5 mm in width and 5 mm in depth, and separated at a centre-to-centre distance of 20 mm. The other type of substrate (**b**) had grooves of 1 mm in width and 1 mm in depth (Fig. 9). The separations between grooves were 20 mm in all cases. The reverse face and side ends were coated with insulating paint. The substrate was positioned in an electroplating cell so that longitudinal axes of the grooves were in the vertical direction. The anode was a copper plate of $125\,cm^2$ and was positioned at a distance of 10 cm from the cathode. The electroplating cell was rectangular in shape (length × width × depth = 170mm × 135mm × 120mm

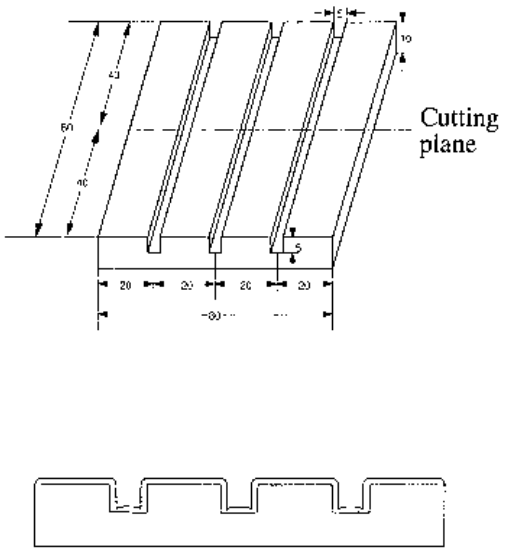

Fig. 8. Outline of a steel substrate (top) and its cross section (bottom). The size is given in millimetres.

in inner size). A stirring bar of 40 mm was magnetically rotated at 330 rpm at the bottom centre. The position of the substrate (cathode) was 40 mm from the centre (rotation axis of stirring bar). The cell was thermostated at 60 °C. After the plating the cathode was cut in perpendicular to the grooves. The cross section, which is schematically shown in Fig. 8, was observed under a microscope. The thickness of deposit was measured on photomicrographs of the cross section.

Polarization measurements were performed using a copper plate of 80 mm × 80 mm, instead of a steel substrate, under otherwise the same conditions.

5.2. *Results*

Copper plating was performed on substrate **a** at a current density of $10\,mA\,cm^{-2}$ based on the geo-

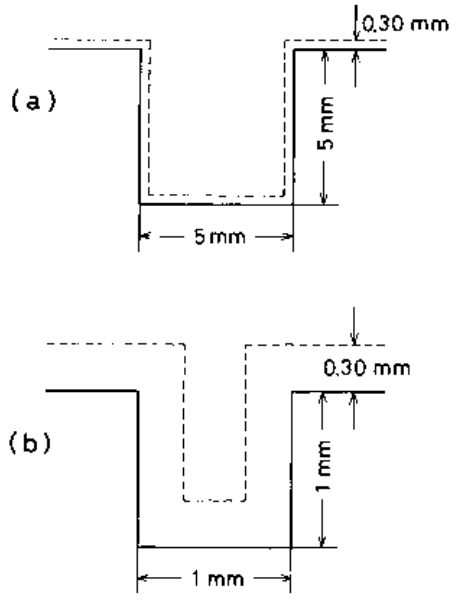

Fig. 9. Geometry of two types substrates. Thin broken lines indicate the estimated thickness of diffusion layer (see Section 5.2).

metric area of the cathode (including the surface area in grooves). After 80 min, the cathode was cut and the cross section was observed under a microscope. Figure 10 shows examples of photomicrographs of the cross section. The thicknesses of the copper deposit measured at different locations are summarized in Table 1. The locations are indicated by the distance, measured in units of (5/8) mm, from a reference point. The copper coating was relatively uniform, although it was thinner at the bottom corner, and thicker at the upper edge of the groove. Table 2 shows similar results obtained for substrate **b**.

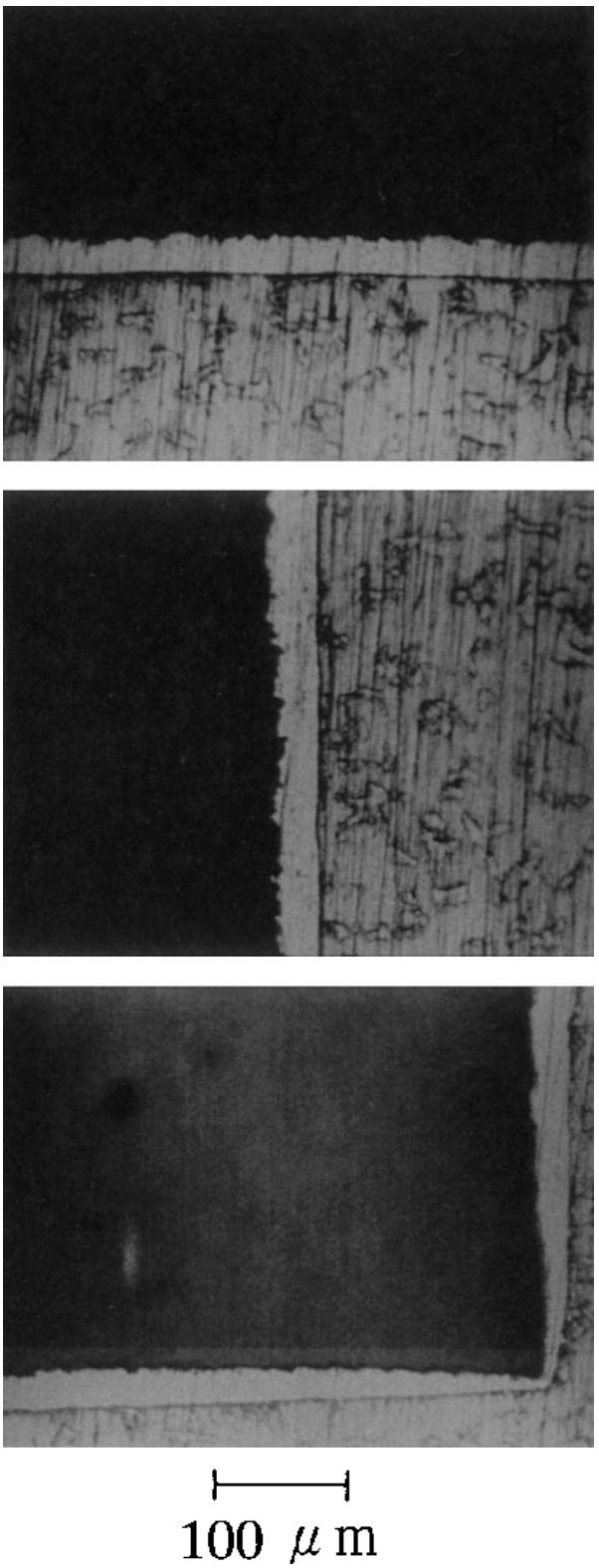

Fig. 10. Photomicrographs of the cross sections of the outer surface (top), side wall of groove (middle), and lower corner of groove (bottom). The layer with light colour is the copper deposit.

Figure 11 shows the results of polarization measurements. The solid line represents the theoretical polarization curve best-fitted to the experimental data ($D/d = 3.5 \times 10^{-4}\,\mathrm{cm\,s^{-1}}$). The polarization curve is a little different from that obtained in the previous measurements (○ in Fig. 7), because the cell geometry and hydrodynamic conditions are different. A diffusion layer thickness of $d = 0.030\,\mathrm{cm}$ was obtained with $D = 1.03 \times 10^{-5}\,\mathrm{cm^2 s^{-1}}$. The polarization curve can be approximated by

$$E = -0.34\ \log\ (i/\mathrm{mA\,cm^{-2}}) - 2.02 \qquad (36)$$

5.3. *Calculation of current distribution of grooved substrates*

The thickness of diffusion layer (d) depends on the configuration of substrate and on the hydrodynamic conditions of solution. However it is difficult to estimate the variation of d on the surface of grooved substrates. In the present discussion, therefore, d is assumed to be constant on the whole surface of substrate. The value of $d = 0.030\,\mathrm{cm}$ is adopted in stirred solutions according to the preceding discussion (Section 5.2). The thin broken lines in Fig. 9 indicate the diffusion layer on two types of substrates.

Table 1. Thickness of deposit on substrate ***a*** *with 5 mm × 5 mm grooves*

Location	*Thickness of deposit / μm*
Bottom of the groove*	
0.5	33.3
1.5	32.2
2.5	30.0
3.5	25.6
Side wall of the groove†	
0.5	26.1
1.5	26.7
2.5	27.8
3.5	30.0
4.5	32.2
5.5	33.3
6.5	35.0
7.5	38.9
Outer surface‡	
0.5	42.7
1.5	40.8
2.5	38.9
3.5	36.7
4.5	36.7
10.5	36.7
11.5	36.7

Current density, 10 mA cm^{-2}; time, 80 min.
* Distance in (5/8) mm from the centre of groove
† Distance in (5/8) mm from the bottom of groove
‡ Distance in (5/8) mm from the edge of groove

Table 2. Thickness of deposit on substrate **b** *with 1 mm × 1 mm grooves*

Location	*Thickness of deposit* / μm
Bottom of the groove*	
1.0	13.9
2.0	10.5
3.0	9.4
4.0	8.3
Side wall of the groove†	
1.0	6.7
2.0	7.2
3.0	7.8
4.0	8.9
6.0	10.6
7.0	11.1
8.0	12.2
Outer surface‡	
1.0	16.7
2.0	19.4
3.0	22.2
5.0	21.7
7.0	22.2

Current density, 10 mA cm^{-2}; time, 40 min.
* Distance in (1/10) mm from the centre of groove
† Distance in (1/10) mm from the bottom of groove
‡ Distance in (1/10) mm from the edge of groove

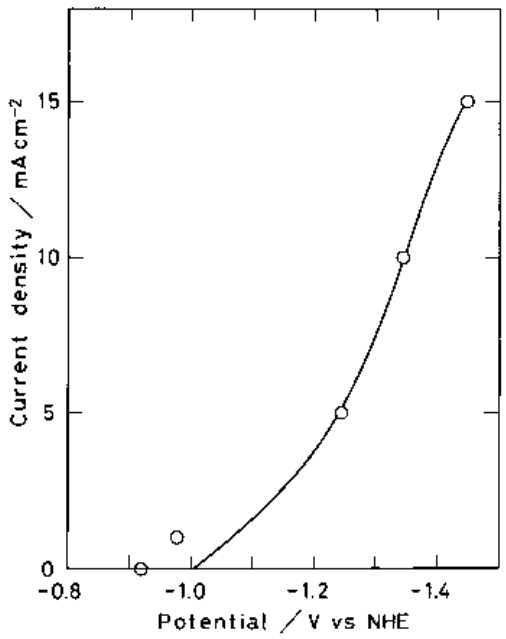

Fig. 11. Current–potential relationship obtained under the same conditions as in electroplating. The solid line is a theoretical curve for $D/d = 3.5 \times 10^{-4}$ cm s^{-1}.

Although this model is a rough approximation, subsequent calculations will provide an insight into the current distribution of copper deposition.

In the case of substrate **a** the diffusion layer is thin in comparison with the size of the groove. Then the current distribution can be calculated assuming uniform resistivity of the solution and empirical current–potential relationship (Equation 36): the so-called secondary distribution arises. The procedure of calculation has been reported in a previous paper [18].

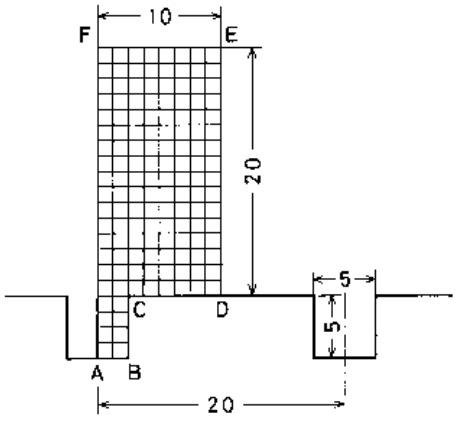

Fig. 12. Cross section of substrate **a**. The meshed area indicates the region in which two-dimensional calculation was performed.

Figure 12 shows the region of numerical calculation of potential. The thickness of the copper deposit was calculated from the current distribution on the basis of Faraday's law. The result is shown by the solid lines in Fig. 13. The thickness of deposit is plotted in the direction normal to the surface of substrate. Figure 13 also includes the experimental data (○) of Table 1 and the theoretical curve (broken line) calculated from the primary current distribution. The experimental data are in fair agreement with the secondary distribution.

In the case of substrate **b**, concentrations and potential were calculated in the diffusion layer using two-dimensional forms of Equations 22, 23, 24 and 28 in combination with the Nernst equation (Equation 9) as the boundary condition at the cathode surface. The potential in the bulk region was calculated assuming uniform resistivity of solution. The thickness of the copper deposit was calculated from the current distribution, and is shown by the solid lines in Fig. 14. Figure 14 also shows the experimental data (○) of Table 2 and the theoretical curve (broken lines) based on primary distribution. The present model explains the experimental data better than the primary distribution, although agreement is not very good. A possible cause for the discrepancy is that the convection may not occur efficiently in this small groove (1 mm × 1 mm). The assumption of uniform thickness of the diffusion layer seems inappropriate. It is necessary to evaluate the effect of convection properly.

6. Conclusions

From theoretical and experimental studies, the following conclusions have been drawn:
(i) The equilibrium potential of the copper electrode in CuCN–KCN solutions can be expressed as a function of the CN/Cu ratio.
(ii) When copper is deposited at the cathode, concentration polarization occurs due to the liberation of CN^- ions.
(iii) Potential and concentration distributions can be calculated by taking into account the diffusion and migration of all ionic species, and chemical reactions involving cyano-copper(I) complexes.

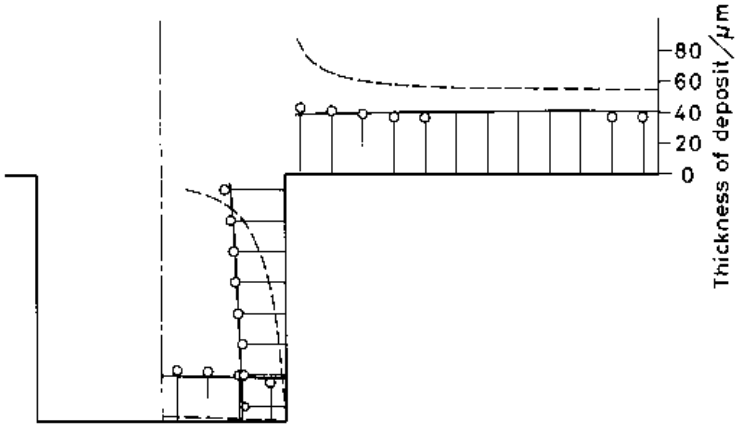

Fig. 13. Distribution of the thickness of copper deposit on substrate **a**. Average current density = 10 mA cm^{-2}, time = 80 min, κ = 0.195 S cm^{-1}. The mark ○ indicates experimental data of Table 1. The solid line corresponds to the secondary current distribution obtained with the empirical current–potential relationship of Equation 36. The broken line represents the primary distribution.

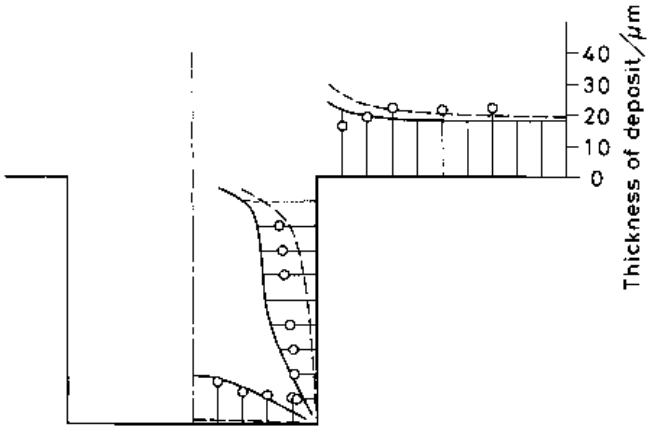

Fig. 14. Distribution of the thickness of copper deposit on substrate **b**. Average current density = 10 mA cm^{-2}, time = 40 min, $c_M^0 = 0.56$ M, $c_A^0 = 2.10$ M, $c_S^0 = 1.54$ M, $T = 333$ K, $\kappa = 0.195$ S cm^{-1}, $\beta_2 = 1.8 \times 10^{22}$, $\beta_3 = 3.8 \times 10^{25}$, $\beta_4 = 1.1 \times 10^{27}$. The mark ○ indicates experimental data of Table 2. The broken line represents the primary distribution.

(iv) Theoretical polarization curve can be obtained by assuming the quasiequilibrium of charge-transfer reaction. The latter assumption is verified by examining kinetic data and experimental polarization curves.
(v) Experimental results of copper deposition in relatively large grooves agree with the secondary current distribution calculated with the empirical current potential relationship.
(vi) When the size of the groove is comparable to the diffusion layer thickness, the present model can not predict experimental results very well. Convective mass transfer in the groove must be considered properly.

Acknowledgement

We are grateful to Prof. Y. Ogata of Kyoto University for valuable comments.

References

[1] N. Ibl,'Comprehensive Treatise of Electrochemistry', Vol. 6, Plenum Press, New York (1983), pp. 1–63, pp. 239–315.
[2] F. Hine, 'Electrode Processes and Electrochemical Engineering', Plenum Press, New York (1985).
[3] J. Newman, 'Electrochemical Systems', 2nd edn, Prentice-Hall, Englewood Cliffs, NJ (1991).
[4] S. Glasstone, *J. Chem. Soc*. (1929) 702.
[5] Y. Kuwa and S. Hayashi, *Kinzoku Hyomen Gijutsu* **12** (1961) 438.
[6] Y. Kuwa, S. Hayashi and M. Oita, *Kinzoku Hyomen Gijutsu* **13** (1962) 10.
[7] H. Gerischer, *Z. Elektrochem.* **57** (1953) 604.
[8] H. Gerischer, *Chemie-Ing.-Techn.* **36** (1964) 666.
[9] M. Costa, *J. Rech. CNRS*. **64** (1963) 285.
[10] R. Yu. Bek and B. D. Zhukov, *Soviet Electrochem.* **12** (1976) 1291.
[11] R. E. Sinitski, V. Srinivasan and R. Hayens, *J. Electrochem. Soc.* **127** (1980) 47.
[12] R. Ruffoni and D. Landolt, *Electrochim. Acta* **33** (1988) 1281.
[13] A. Katagiri, *J. Appl. Electrochem.* **21** (1991) 487.
[14] A. Katagiri, H. Inoue and N. Ogure, Abstract No. 3C27, presented at the 59th Meeting of the Electrochemical Society of Japan, Hachioji, 2–4 April (1992).
[15] A. Katagiri, Proceedings of the Symposium on New Mathematical and Computational Methods in Electrochemical Engineering PV 93–14, The Electochemical Society (1993), p. 203.
[16] R. A. Penneman and L. H. Jones, *J. Chem. Phys.* **24** (1956) 293.
[17] A. J. Bard and L. R. Faulkner, 'Electrochemical Methods', Wiley & Sons, New York (1980).
[18] A. Katagiri and Y. Miyazaki, *J. Appl. Electrochem.* **19** (1989) 281.
[19] W. L. Latimer, 'The Oxidation States of the Elements and their Potentials in Aqueous Solutions', 2nd edn, Prentice-Hall, Englewood Cliffs, New York (1952).
[20] J. Kielland, *J. Am. Chem. Soc*. **59** (1937) 1675.

Appendix A: Temperature dependence of β_m^a

Thermodynamic formation constants β_m^a (in terms of activities) for Reactions 2–4 at a temperature T are calculated from

$$\ln \beta_m^a(T) - \ln \beta_m^a(298.15) = -(\Delta H_m^0/R)(1/T - 1/298.15) \quad \text{(A1)}$$

where the standard enthalpy changes for Reactions 2–4 are estimated to be $\Delta H_2^0 = -52\,\mathrm{kJ\,mol^{-1}}$, $\Delta H_3^0 = -136\,\mathrm{kJ\,mol^{-1}}$, and $\Delta H_4^0 = -186\,\mathrm{kJ\,mol^{-1}}$, as follows.

The standard Gibbs energy change ΔG_4^0 for Reaction 4 at 298.15 K is calculated from β_4^a ($= 2 \times 10^{30}$) as

$$\Delta G_4^0 = -RT \ln \beta_4^a = -173\,\mathrm{kJ\,mol^{-1}}$$

Since $Cu(CN)_4^{3-}$ has the same tetrahedral geometry as $Zn(CN)_4^{2-}$ and $Hg(CN)_4^{2-}$, the standard entropy change ΔS_4^0 for Reaction 4 may be similar to that of reactions

$$Zn^{2+} + 4CN^- \longrightarrow Zn(CN)_4^{2-}$$
$$Hg^{2+} + 4CN^- \longrightarrow Hg(CN)_4^{2-}$$

for which $\Delta S^0 = -44.4\,\mathrm{J\,K^{-1}}$ and $\Delta S^0 = -49.4\,\mathrm{J\,K^{-1}}$ have been reported [19]. Assuming the former value ($\Delta S_4^0 = -44.4\,\mathrm{J\,K^{-1}}$), the standard enthalpy change for Reaction 4 can be estimated as

$$\Delta H_4^0 = \Delta G_4^0 + (298.15)\Delta S_4^0 = -186\,\mathrm{kJ\,mol^{-1}}$$

The following values of ΔH^0 have been reported [16]:

$$Cu(CN)_3^{2-} + CN^- \longrightarrow Cu(CN)_4^{3-} \qquad \Delta H_{3,4}^0 = -50\,\mathrm{kJ\,mol^{-1}}$$
$$Cu(CN)_2^- + CN^- \longrightarrow Cu(CN)_3^{2-} \qquad \Delta H_{2,3}^0 = -84\,\mathrm{kJ\,mol^{-1}}$$

Therefore, the standard enthalpy change for Reactions 3 and 2 are estimated as

$$\Delta H_3^0 = \Delta H_4^0 - \Delta H_{3,4}^0 = -136\,\mathrm{kJ\,mol^{-1}}$$
$$\Delta H_2^0 = \Delta H_3^0 - \Delta H_{2,3}^0 = -52\,\mathrm{kJ\,mol^{-1}}$$

For example, the values of β_m^a at 60 °C are $\beta_2^a = 1.1 \times 10^{23}$, $\beta_3^a = 1.2 \times 10^{26}$, and $\beta_4^a = 7.4 \times 10^{26}$.

Appendix B: Formation constants in terms of concentrations

Formation constants β_m of $Cu(CN)_m^{(m-1)-}$ (in terms of concentrations) are related to thermodynamic formation constants β_m^a (in terms of activities) by

$$\beta_m = \beta_m^a(\gamma_{Cu^+})(\gamma_{CN^-})^m/(\gamma_{Cu(CN)_m^{(m-1)-}}) \quad \text{(B1)}$$

where γ_i is the activity coefficient of ion i.

According to the Debye–Hückel theory, γ_i is expressed as

$$\log_{10}\gamma_i = -Az_i^2 I^{1/2}(1 + Ba_i I^{1/2}) \quad \text{(B2)}$$

where I is the ionic strength ($\mathrm{mol\,dm^{-3}}$) and a_i is the ion size parameter (Å). A and B are constants: $A = 0.504$ (15 °C), 0.517 (30 °C), 0.550 (60 °C); $B = 0.327$ (15 °C), 0.330 (30 °C), 0.337 (60 °C). The following values of a_i are adopted: $a_{Cu^+} = 2.5$ Å (estimated from $a_{Ag^+} = 2.5$ Å [20]), $a_{CN^-} = 3.7$ Å [16], $a_{Cu(CN)_2^-} = a_{Cu(CN)_3^{2-}} = a_{Cu(CN)_4^{3-}} = 6.6$ Å [16].

Ionic strength I of a solution prepared from CuCN and KCN is calculated according to the stoichiometry of the following reactions:

$$CuCN + KCN = K^+ + Cu(CN)_2^-$$
$$CuCN + 2KCN = 2K^+ + Cu(CN)_3^{2-}$$
$$CuCN + 3KCN = 2K^+ + Cu(CN)_4^{3-}$$

Thus,

$$I = 2c_A - 3c_M \quad \text{for } 2 \le c_A/c_M \le 3$$
$$I = 3c_A - 6c_M \quad \text{for } 3 \le c_A/c_M \le 4$$
$$I = c_A + 2c_M \quad \text{for } c_A/c_M \ge 4$$

For example, the following values of γ_i and β_m are obtained for $c_M = 0.56$ M, $c_A = 2.10$ M, and $c_S = 1.54$ M at 60 °C: $\gamma_{Cu^+} = 0.412$, $\gamma_{CN^-} = 0.501$, $\gamma_{Cu(CN)_2^-} = 0.637$, $\gamma_{Cu(CN)_3^{2-}} = 0.165$, $\gamma_{Cu(CN)_4^{3-}} = 0.0181$, $\beta_2 = 1.8 \times 10^{22}$, $\beta_3 = 3.8 \times 10^{25}$, $\beta_4 = 1.1 \times 10^{27}$.

Appendix C: Calculation of diffusion coefficient from conductivity data

Diffusion coefficient D_i and molar conductivity λ_i of ion i are related by the Nernst–Einstein equation:

$$D_i = RT\lambda_i/z_i^2F^2 \quad \text{(C1)}$$

Using Equation C1, the conductivity of solution κ is expressed as

$$\kappa = \sum \lambda_i c_i = (F^2/RT)\sum z_i^2 D_i c_i$$

Assuming that all D_i values are identical ($D_i = D$), we obtain the following equation:

$$\kappa = (F^2 D/RT)\sum z_i^2 c_i$$

Therefore,

$$D = \kappa RT/(F^2 \sum z_i^2 c_i) \quad \text{(C2)}$$

For a given solution of CuCN–KCN at temperatue T, values of c_{CN}, c_2, c_3, and c_4 can be calculated from Equations 5–7 using estimated β_m (see Appendixes A and B). For example, for $c_M = 0.56$ M, $c_A = 2.10$ M, and $c_S = 1.54$ M at 60 °C, concentrations of K^+, CN^-, $Cu(CN)_2^-$, $Cu(CN)_3^{2-}$, and $Cu(CN)_4^{3-}$ are calculated to be 1.54, 6.25×10^{-2}, 1.47×10^{-3}, 0.197 and 0.359 M, respectively. Introducing these values and experimental data of $\kappa = 0.195\,\mathrm{S\,cm^{-1}}$ into Equation C2 gives $D = 1.03 \times 10^{-5}\,\mathrm{cm^2\,s^{-1}}$. Similarly, $D = 4.67 \times 10^{-6}\,\mathrm{cm^2\,s^{-1}}$ is obtained from $\kappa = 0.106\,\mathrm{S\,cm^{-1}}$ at 15 °C.